CROSSTALK EFFECT IN NOAA-20 VIIRS THERMAL EMISSIVE BANDS

Junqiang Sun[1] and Xiaoxiong Xiong[2]

[1]Science Systems and Applications Inc., 10210 Greenbelt Road, Suite 600, Lanham, MD 20706.
[2]Sciences and Exploration Directorate, NASA/GSFC, Greenbelt, MD 20771, USA

ABSTRACT

Crosstalk contamination in the Moderate Resolution Imaging Spectroradiometer (MODIS) thermal emissive bands (TEBs) has been a known issue since prelaunch, that has amplified on-orbit for some of bands. A linear algorithm has been developed and successfully applied to mitigate the crosstalk effect and restore the quality and accuracy of the MODIS L1B products. Significant crosstalk effect has also been found and characterized in TEBs of the Visible Infrared Imaging Radiometer Suite (VIIRS) on the Suomi National Polar-orbiting Partnership (SNPP). NOAA-20 VIIRS, a follow-on instrument to SNPP VIIRS, was launched on November 18, 2017. In this report, it is shown that there are nonnegligible crosstalk contaminations among the TEBs of NOAA-20 VIIRS as well. They are characterized using the scheduled lunar observations and compared with those in SNPP VIIRS.

Index Terms— Calibration, Radiometry, Remote Sensing

1. INTRODUCTION

The NOAA-20 Visible Infrared Imaging Radiometer Suite (VIIRS), a follow-on instrument to the Suomi National Polar-orbiting Partnership (SNPP) VIIRS, was successfully launched on November 18, 2017. VIIRS has 22 spectral bands, among which fourteen are reflective solar bands (RSBs) and seven are thermal emissive bands (TEBs) [1,2]. The TEBs cover a spectral range from 3.70 to 12.013 μm and are calibrated using an on-board blackbody (BB) [3,4]. A quadratic form is used to relate the top of atmosphere (TOA) radiance and background subtracted instrument response for the TEBs. The offset and the nonlinear terms are monitored by the annually scheduled BB warm-up-cool-down (WUCD) measurements whereas the linear term is calculated on a scan-by-scan basis.

Serious crosstalk contaminations have been found in both Terra and Aqua MODIS [5-8], especially in the Terra MODIS long wave infrared bands [5-7]. Significant crosstalk effect has also been identified in SNPP VIIRS TEBs [9]. The crosstalk effect induces unexpected sudden jumps, rapid changes, and strong detector differences in the calibration coefficients, striping and ghosting in the Earth view (EV) imagery, and long-term drifts in the EV retrievals [5-7]. The artifacts induced in the Level 1B (L1B, MODIS) or sensor data records (SDR, VIIRS) products, if uncorrected, propagate to higher level of science products, resulting in large errors, failure of the algorithms, and erroneous scientific conclusions. Sun et al. [5,6] have developed a linear model to describe the crosstalk effect and have shown a successful mitigation of the artifacts in both the calibration coefficients and L1B products, as well as restoration of the accuracy of the science products.

In this paper, it is shown that there is a nonnegligible crosstalk effect in NOAA-20 VIIRS TEBs. The crosstalk contaminations among the NOAA-20 VIIRS TEBs are also quantitatively characterized by using the regularly scheduled lunar observations [9]. The rest of the paper is organized as follows: In Section 2, the crosstalk effect for the affected TEBs is demonstrated using lunar images. In Section 3, the crosstalk correction methodology and the crosstalk characterization algorithm are briefly reviewed. In Section 4, the crosstalk coefficients are derived for the affected TEBs from the scheduled lunar observations and the results are discussed and compared with SNPP VIIRS. Section 5 is a brief summary of this analysis.

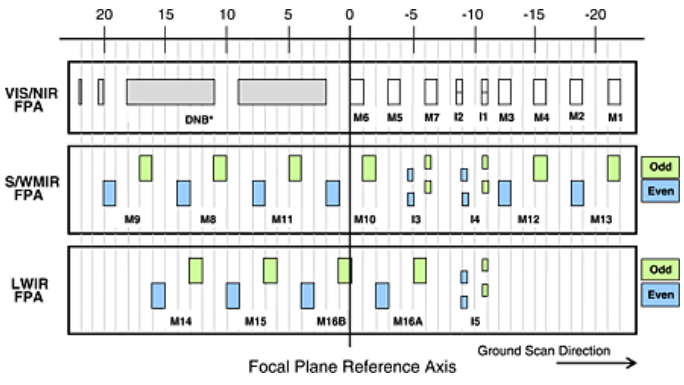

Fig. 1. VIIRS Focal Plane Assembly.

2. CROSSTALK EFFECT IDENTIFICATION

There are two types of crosstalk contaminations. One is electronic crosstalk, while the other is optical crosstalk. Electronic crosstalk in a remote sensing instrument is a phenomenon causing electronic signals to be induced into a particular band from the detectors of neighboring bands on the same FPA. The optical crosstalk is optical communication between bands via the spectral filter array, which also only occurs among the bands on the same FPA. VIIRS has three FPAs, visible and near-infrared (VIS/NIR), short and middle infrared (S/MIR), and long-wave infrared (LWIR), which are shown in Fig. 1. Both electronic and optical crosstalk induce ghost images due to the different locations of the receiving and sending bands on the FPA, resulting in different times for them to view a same target [5,8]. The ghost images of a target with sharp edges can then be used to identify, as well as to characterize the crosstalk effect [5,6].

The Moon is a "point-like" target with a finite size and a clear edge profile [5,9] that can be used to identify and characterize the crosstalk effect. For NOAA-20 VIIRS, the instrument has been regularly scheduled to observe the Moon approximately monthly since its launch [10]. So far, there are already seventeen scheduled lunar observations since November 2017. If there is no crosstalk effect in a detector of a spectral band, the lunar image observed by the detector is cylindrical in shape with a clear edge profile, else ghost features such as hills, long tails, and valleys around the edge of the lunar image can be seen [5,6,8].

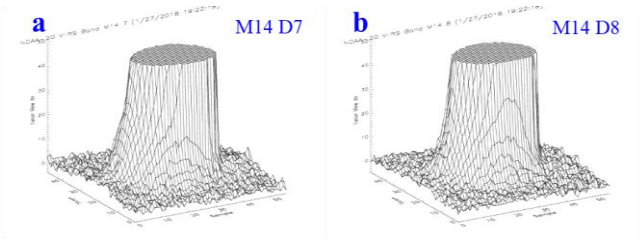

Fig. 2. Lunar images observed by SNPP VIIRS band M14 on 27 January 2018 for (a) Detector 7 and (b) Detector 8.

Fig. 2 shows two lunar images observed by band M14 detector 7 and 8, respectively, on January 27, 2018. They both have very clear and sharp edges at right side, while there are observable tails on the left side of the both images. This means that there is no crosstalk contamination on the right side of the lunar images, but there are clear crosstalk contaminations on the left side of the images. From Fig. 1, it is seen that band M14 is located at the left end of the LWIR FPA. All other LWIR bands are located on its right side. According to arrow for the ground scan direction in Fig. 1, all other LWIR bands view the Moon before band M14 in each scan. Then if there is any crosstalk contamination, it should show up around the left side edge of the lunar image. In other words, the tails in the two lunar images are the crosstalk contaminations from other LWIR bands on the LWIR FPA. By carefully examining the two lunar images, it can be seen that tail in the lunar image of the detector 7 is a little bit larger than that of the detector 8. In other words, detector 7 of the band M14 has larger crosstalk effect than detector 8. By viewing the lunar images of all detectors of band M14, we can conclude that there is a noticeable crosstalk effect in all M14 detectors and the crosstalk contamination in the odd numbered detectors is larger than those with even numbered detectors.

We have also examined the lunar images for detectors for all other TEBs and found that bands M13, M15 and M16 also exhibit noticeable crosstalk contamination of a similar magnitude as band M14, while bands M12, I4, and I5 have smaller magnitudes compared to those in bands M13-M16.

3. CROSSTALK CORRECTION ALGORITHM

As mentioned previously, there are two types of crosstalk, i.e., optical crosstalk and electronic crosstalk. The optical crosstalk from a sending band can be linearly related to the instrument response of the sending band due to the property of the optical communication. Electronic crosstalk is a much more complex phenomenon. As a first approximation, the electronic crosstalk can also be described using a linear relationship between the crosstalk contamination from a sending band and its instrument response. This linear approximation has been validated in MODIS TEBs which are significantly contaminated by crosstalk effect [5-8]. The optical crosstalk and electronic crosstalk cannot be separated from on-orbit measurements as they induce same phenomena even though electronic crosstalk can have negative contribution while optical crosstalk cannot. However, there is no need to separate them for mitigating their effects in science product applications. Then we can relate the crosstalk contaminations including both optical and electronic crosstalk contributions in a receiving band to the signals in the sending bands by [9]

$$dn^{xtalk}_{B_r,D_r}(F) = \sum_{B_sP_s} C(B_r, D_r, B_s, P_s)\langle dn^{msr}_{B_sD_s}(F + F_{B_rP_r} - F_{B_sP_s}\rangle_{P_s} \quad , \quad (1)$$

where B_r, D_r, and B_s, represent the receiving band, receiving detector, and sending band, respectively, P_r is the parity of detector D_r, P_s is the detector parity of sending band B_s, F is the pixel number along scan of band B_r, F_{BD} is the pixel shift between band B detector D and the focal plane reference axis, the brackets indicate the average over the detectors with parity P_s of the sending band B_s, $C(B_r,D_r,B_s,P_s)$ is the effective crosstalk coefficient from the sending band B_s detectors with parity P_s to the receiving band B_r detector D_r, and *msr* indicates that the instrument response *dn* is the measured one before crosstalk correction. Eq. (1) requires that the pixel sizes of the receiving band and sending bands are the same and that F_{BD} is counted consistently based on the pixel size.

The key step in removing the crosstalk effect in an affected band is to obtain the crosstalk coefficients. Eq. (1) can be applied to an area within an image, within which the signals are primarily contaminated with crosstalk to derive the coefficients. So far, the edges of the lunar images are known to be the most optimal for this purpose [5,6,8,9]. With the crosstalk coefficients derived from the lunar observations, the crosstalk contaminations can be calculated using either Eq. (1), and then subtracting them from the measured signals of the band in both BB calibration, including routine and WUCD measurements and EV observations [5-9].

4. CROSSTALK COEFFICENTS

The lunar images are known to be the most optimal for deriving the crosstalk coefficients as mentioned previously [5,6,8]. To derive C(Br,Dr,Bs,Ps) using Eq. (1), the summation of the dn over scans for each given frame or sample along-scan instead of dn is needed since the lunar surface is not uniform [5]. In this analysis, we will focus on the coefficients C(Br,Dr,Bs,Ps). The details of the crosstalk coefficients derivation from the lunar observations has been well described in our previous work [5,6,8,9].

From the lunar imagery analysis, we can identify the primary sending band for each affected band. In the following, we will concentrate on bands M13-M16 since they have larger crosstalk effects compared to other three bands M12, I4, and I5. It is worth mentioning that most NOAA-20 VIIRS TEBs saturate when they view the brightest part of lunar surface. A scaling scheme is applied to estimate the instrument response at the saturated region for each band using a corresponding image of an unsaturated band to reconstruct the response (dn) in the saturated region via a scaling [5,8].

As already demonstrated in Section 2, the band M14 receives crosstalk contamination from the bands located to its right side on the LWIR FPA. There are three such bands − M15, M16 (M16A and M16B), and I5 − to the right of band M14 and they in principle can have crosstalk with band M14. The analysis of the tails at the left side of the lunar images for the band M14 reveals that there are no crosstalk contaminations from bands M16 and I5 or that the contributions from them are negligible. Thus, the crosstalk contaminations as demonstrated by the tails at the left side of the lunar images shown in Fig. 2 come from the band M15. Figure 3 shows the crosstalk coefficients derived from the band M14 lunar observations for the first six months of operation. In the plot, the coefficients are expressed in percentages. It is easy to see that there are no visible long-term changes in the coefficients, although fluctuations are obvious. The fluctuations are considered to come from the remaining uncertainties of the estimation, which are not significant in the context of this analysis. Figure 3a shows the crosstalk coefficients for all detectors of the band M14 from the odd detectors of the band M15. It is easy to see that the coefficients fall into two separate groups, based on the evenness or the oddness, or parity, of the detectors. The coefficients for the crosstalk contaminations in the band M14 for its odd detectors are about 0.25%, while those for the even detectors are close to 0.15%. This is consistent with the fact that the odd detectors are located closer to the band M15. Figure 3b shows the crosstalk coefficients for all detectors of the band M14 from the even detectors of the band M15. Once again, the coefficients fall into two groups, one for the odd detectors and the other for the even detectors. For odd detectors, the crosstalk coefficients are about the same, and are close to ~0.4%. For even detectors, they are much smaller at close to ~0.05%. As mentioned previously, it is difficult to separate the effect of electronic crosstalk and optical crosstalk. In other words, it is difficult to identify whether the crosstalk effect in the band M14 is induced by electronic crosstalk or optical crosstalk. Nevertheless, the dependence of the crosstalk effect on the distance between a receiving detector and a sending detector indicates that the crosstalk is most likely optical crosstalk. But the distance dependency is not as clearly observed as in SNPP VIIRS TEBs [9]. Also, the electronic crosstalk effect may also play a significant role in the case of NOAA-20 VIIRS band M14.

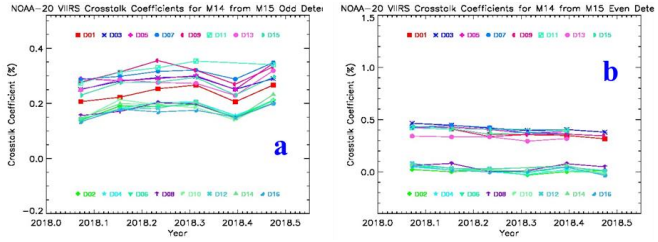

Fig. 3. NOAA-20 VIIRS band M14 crosstalk coefficients for the sending band M15 for (a) odd detectors and (b) even detectors.

Similarly, we have derived the crosstalk coefficients for bands M13, M15 and M16 and can derive them for bands M12, I4, and I5 as well. Their crosstalk coefficients have similar patterns and features as those of bands M13 and M14 shown in Fig. 3 and also do not have indicate any time dependence.

As demonstrated and discussed above, the crosstalk coefficients of NOAA-20 VIIRS TEBs have no distinct temporal dependence. This is consistent to what was observed in SNPP VIIRS [8]. Since the crosstalk coefficients for the TEBs are stable, we can average them over time to get a set of static crosstalk coefficients. Figure 4 shows the time-averaged crosstalk coefficients for the odd and even detectors of the sending bands, respectively, for NOAA-20 VIIRS bands M13-M16. Since the EV temperature is relatively smooth over a few kilometers, the signals in the odd and even detectors for a TEB expectedly are about the same. Thus, we can further sum up the averaged coefficients in Fig. 4 for each individual receiving detector and band for comparison purpose. Figure 5a shows the summations of the averaged crosstalk coefficients in Figs. 4a and 4b. First, we can see that the crosstalk contaminations in bands M13, M14, and M16 are about the same level, while those in the band M15 are reduced by a factor of 2. Second, there is a very clear difference between the odd and even detectors in all the four bands. Third, bands M14 and M15 have the same odd-even pattern, while bands M13 and M16 show an opposite odd-even pattern. Figure 5b shows the summations of the crosstalk coefficients for SNPP VIIRS bands M13-M16. By comparing Figs. 5a and 5b, it can be seen that the total crosstalk contamination in NOAA-20 VIIRS bands M13, M15, and M16 are about the same level as their counterparts in SNPP VIIRS, while the NOAA-20 VIIRS band M14 has much less crosstalk effect compared to the SNPP VIIRS band M14.

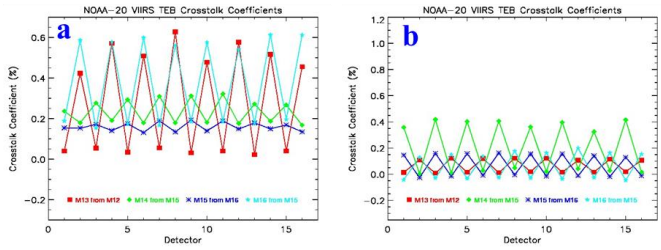

Fig. 4. Crosstalk coefficients for NOAA-20 VIIRS bands M13-M16: (a) odd detectors and (b) even detectors.

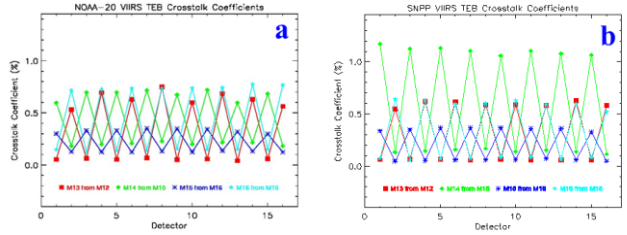

Fig. 5. Crosstalk coefficients for VIIRS bands M13-M16 for (a) NOAA-20 and (b) SNPP.

The odd-even detector difference observed in both NOAA-20 and SNPP VIIRS TEBs definitely can induce the currently known pattern in the calibration coefficients derived from the BB calibration and scene-dependent striping in its EV retrievals for each of the four bands. Because the crosstalk effect depends on the signals of the sending bands, its impact on the EV retrievals can be further intensified in the WUCD calibration during which the BB temperature is raised. The reported artifacts appearing in the SST during the WUCD time periods [4] are consistent with this finding.

The crosstalk effect in VIIRS TEBs on both NOAA-20 and SNPP are smaller compared to those in MODIS LWIR PV bands, in which the crosstalk effect is not only strong but also becomes increasingly more severe with time [5-7]. Nevertheless, the VIIRS TEBs crosstalk effect for both NOAA-20 and SNPP is non-negligible [9] and the features of the crosstalk contaminations match the properties of the artifacts [4]. A direct connection of these observed artifacts to the crosstalk contaminations in the two instruments is yet to be explicitly demonstrated, and the mitigation awaits further effort.

5. SUNMARY

Crosstalk contaminations in NOAA-20 VIIRS TEBs have been examined and characterized using the scheduled lunar observations. The crosstalk coefficients derived from the lunar observations for bands M13-M16 are presented and analyzed. They are dependent on both the specific band and detector. The crosstalk contaminations in these bands are about the same level

compared to those in their counterparts in SNPP VIIRS. They are smaller than those observed in MODIS LWIR bands, but large enough to induce significant impact on the EV retrievals of these bands. A clear difference between the odd and even detectors for the affected bands is demonstrated, and this detector-based difference can induce striping in the EV imagery.

ACKNOWLEDGMENTS

We would like to thank Amit Angal for his valuable comments and suggestions.

REFERENCES

[1] C. Schueler, J. E. Clement, P. Ardanuy, C. Welsh, F. DeLuccia, and H. Swenson, NPOESS VIIRS sensor design overview, Proc. SPIE 4483, 11-23 (2001).

[2] C. Cao, F. Deluccia, X. Xiong, R. Wolfe, and F. Weng, Early on-orbit performance of the Visible Infrared Imaging Radiometer Suite (VIIRS) onboard the Suomi National Polar-orbiting Partnership (S-NPP) satellite, IEEE Trans. Geosci. Remote Sens. 52, 1142–1156 (2014).

[3] Y. Li, X. Xiong, J. McIntire, A. Angal, S. Gusev, and K. Chiang "NOAA-20 VIIRS thermal emissive bands on-orbit performance", Proc. SPIE 10781, 107810N (2018)

[4] W. Wang, C. Cao, A. Ignatov, X. Liang, Z. Li, L. Wang, B. Zhang, S. Blonski, J. and Li, Improving the Calibration of Suomi NPP VIIRS Thermal Emissive Bands During Blackbody Warm-up/Cool-Down. IEEE Trans. Geosci. Remote Sens., 57, 1977-1994 (2019).

[5] J. Sun, X. Xiong, S. Madhavan, B. N. Wenny, Terra MODIS band 27 electronic crosstalk effect and its removal, IEEE Trans. Geosci. Remote Sens., 52, 1551–1561 (2014).

[6] J. Sun, X. Xiong, Y. Li, S. Madhavan, A. Wu, B. N. Evaluation of radiometric improvements with electronic crosstalk correction for Terra MODIS band 27. IEEE Trans. Geosci. Remote Sens., 52, 6497–6507 (2014).

[7] J. Sun, S. Madhavan, M. Wang, Crosstalk effect mitigation in black body warm-up cool-down calibration for terra MODIS long wave infrared photovoltaic bands, J. Geophys. Res. Atmos., 121, 8311–8328 (2016).

[8] J. Sun, and M. Wang, Electronic crosstalk in Aqua MODIS long-wave infrared photovoltaic bands. Remote Sen., 8, 806, 1-11 (2016).

[9] J. Sun and M. Wang, Crosstalk effect in SNPP VIIRS, Remote Sen., 9, 344 (2017).

[10] J. Sun and X. Xiong, VIIRS reflective solar bands on-orbit calibration using the Moon, Proc. SPIE 11151, 111511P (2019).